

Article

CAR-NK Cells Targeting HER1 (EGFR) Show Efficient Anti-Tumor Activity against Head and Neck Squamous Cell Carcinoma (HNSCC)

Juliette Nowak ¹, Marco Bentele ¹, Ivana Kutle ¹, Katharina Zimmermann ¹, Jonathan Lukas Lühmann ² , Doris Steinemann ², Stephan Kloess ³, Ulrike Koehl ^{3,4,5}, Willi Roßberg ⁶, Amed Ahmed ⁶, Dirk Schaudien ⁷, Lavinia Neubert ^{8,9}, Jan-Christopher Kamp ^{9,10} , Mark P. Kuehnel ^{8,9}, Athanasia Warnecke ⁶ , Axel Schambach ^{1,11,*} and Michael Morgan ^{1,*}

- ¹ Institute of Experimental Hematology, Hannover Medical School, 30625 Hannover, Germany; nowak.juliette@mh-hannover.de (J.N.); bentele.marco@mh-hannover.de (M.B.); kutle.ivana@mh-hannover.de (I.K.); zimmermann.katharina@mh-hannover.de (K.Z.)
- ² Department of Human Genetics, Hannover Medical School, 30625 Hannover, Germany; luehmann.jonathan@mh-hannover.de (J.L.L.); steinemann.doris@mh-hannover.de (D.S.)
- ³ Institute for Cellular Therapeutics, Hannover Medical School, 30625 Hannover, Germany; kloess.stephan@mh-hannover.de (S.K.); koehl.ulrike@mh-hannover.de (U.K.)
- ⁴ Institute of Clinical Immunology, University Leipzig, 04103 Leipzig, Germany
- ⁵ Fraunhofer Institute for Cell Therapy and Immunology, IZI, 04103 Leipzig, Germany
- ⁶ Department of Otolaryngology, Head and Neck Surgery, Hannover Medical School, 30625 Hannover, Germany; rossberg.willi@mh-hannover.de (W.R.); ahmed.amed@mh-hannover.de (A.A.); warnecke.athanasia@mh-hannover.de (A.W.)
- ⁷ Fraunhofer Institute for Toxicology and Experimental Medicine, ITEM, 30625 Hannover, Germany; dirk.schaudien@item.fraunhofer.de
- ⁸ Institute of Pathology, Hannover Medical School, 30625 Hannover, Germany; neubert.lavinia@mh-hannover.de (L.N.); mkuehnel@ukaachen.de (M.P.K.)
- ⁹ Biomedical Research in Endstage and Obstructive Lung Disease Hannover (BREATH), German Center for Lung Research (DZL), 30625 Hannover, Germany; kamp.jan-christopher@mh-hannover.de
- ¹⁰ Department of Respiratory Medicine, Hannover Medical School, 30625 Hannover, Germany
- ¹¹ Division of Hematology/Oncology, Boston Children's Hospital, Harvard Medical School, Boston, MA 02115, USA
- * Correspondence: schambach.axel@mh-hannover.de (A.S.); morgan.michael@mh-hannover.de (M.M.)



Citation: Nowak, J.; Bentele, M.; Kutle, I.; Zimmermann, K.; Lühmann, J.L.; Steinemann, D.; Kloess, S.; Koehl, U.; Roßberg, W.; Ahmed, A.; et al. CAR-NK Cells Targeting HER1 (EGFR) Show Efficient Anti-Tumor Activity against Head and Neck Squamous Cell Carcinoma (HNSCC). *Cancers* **2023**, *15*, 3169. <https://doi.org/10.3390/cancers15123169>

Academic Editors: Vita Golubovskaya and Walter F. Bodmer

Received: 8 May 2023

Revised: 6 June 2023

Accepted: 8 June 2023

Published: 13 June 2023



Copyright: © 2023 by the authors. Licensee MDPI, Basel, Switzerland. This article is an open access article distributed under the terms and conditions of the Creative Commons Attribution (CC BY) license (<https://creativecommons.org/licenses/by/4.0/>).

Simple Summary: Despite new therapeutic approaches in the last decades, prognosis and survival rates for head and neck squamous cell carcinomas (HNSCC) remain poor. Due to its high immune cell infiltration, immunotherapy has become a valuable tool for HNSCC, yet only three monoclonal antibodies have been approved to treat HNSCC. The aim of this study was to develop novel immunotherapeutic strategies for HNSCC employing CAR-NK cells that target HER1/epidermal growth factor receptor (EGFR), which is overexpressed in over 80% of HNSCC patients. We confirmed CAR-NK cell function by assessing cytotoxic killing, IFN γ secretion and CD107a degranulation in 2D and 3D co-culture models. Analyses of primary HNSCC cells that were still viable after anti-HER1 CAR-NK-92 cell challenge showed a high percentage of CD44v6-positive cells, indicating that targeting HER1 alone was not sufficient to eliminate this potential cancer stem cell population, which could contribute to disease progression such as metastasis. We conclude that CAR-NK cell therapy may be a useful tool for HNSCC treatment in combinatorial therapeutic regimens.

Abstract: (1) Background: HNSCC is a highly heterogeneous and relapse-prone form of cancer. We aimed to expand the immunological tool kit against HNSCC by conducting a functional screen to generate chimeric antigen receptor (CAR)-NK-92 cells that target HER1/epidermal growth factor receptor (EGFR). (2) Methods: Selected CAR-NK-92 cell candidates were tested for enhanced reduction of target cells, CD107a expression and IFN γ secretion in different co-culture models. For representative HNSCC models, patient-derived primary HNSCC (pHNSCC) cell lines were generated by employing an EpCAM-sorting approach to eliminate the high percentage of non-malignant cells found. (3) Results: 2D and 3D spheroid co-culture experiments showed that anti-HER1 CAR-NK-92

cells effectively eliminated SCC cell lines and primary HNSCC (pHNSCC) cells. Co-culture of tumor models with anti-HER1 CAR-NK-92 cells led to enhanced degranulation and IFN γ secretion of NK-92 cells and apoptosis of target cells. Furthermore, remaining pHNSCC cells showed upregulated expression of putative cancer stem cell marker CD44v6. (4) Conclusions: These results highlight the promising potential of CAR-NK cell therapy in HNSCC and the likely necessity to target multiple tumor-associated antigens to reduce currently high relapse rates.

Keywords: chimeric antigen receptor; CAR-NK cells; NK-92 cells; HER1; EGFR; CD44v6; EpCAM; HNSCC; head and neck cancer; immunotherapy

1. Introduction

Head and neck squamous cell carcinomas (HNSCC) are the sixth most common form of cancer worldwide with 380,000 deaths per year globally and a low 5-year survival rate of 40–50% for human papilloma virus (HPV)-negative patients [1,2]. Risk factors for HNSCC development mainly consist of high alcohol and tobacco consumption and HPV infection. The gold standard treatment options to combat HNSCC include combinations of surgery, chemotherapy and radiation. Within the last decades, monoclonal antibodies have been approved as immunotherapeutic approaches to treat HNSCC. For example, cetuximab targets HER1 (epidermal growth factor receptor, EGFR) and showed superior overall survival in recurrent/metastatic (r/m) HNSCC in combination with platinum-based chemotherapy [3]. The approved anti-PD1 immune checkpoint inhibitors (ICI) pembrolizumab and nivolumab showed improved survival rates compared to conventional therapies for r/m HNSCC [4]. However, due to treatment with ICIs, acute toxicities and chronic immune-related adverse events can affect a high number of the patients and limit therapeutic success.

Alternatively, studies with chimeric antigen receptor (CAR) modified immune cells have recently emerged and present highly promising advances in HNSCC due to improved recognition of cancer cells [5–8]. Moreover, a Phase I clinical trial testing a T4-CAR T cell approach targeting the ErbB family demonstrated safe intratumoral administration and stable disease with few adverse effects [9], and additional clinical trials in HNSCC using CAR-T cells targeting MUC1, PD-1, EpCAM and EBV are currently recruiting (NCT05239143, NCT05117138, NCT03740256, NCT05639972, NCT02915445, NCT04847466). While CAR-T cell therapy has shown tremendous success in B cell malignancies, effects in solid tumors have faced multiple challenges, including immunosuppressive tumor microenvironments (TME), choice of target antigens due to intra- and inter-patient tumor heterogeneity, as well as T cell homing and persistence [10]. Furthermore, severe side effects of CAR-T cell therapy were observed in the early clinical trials, including cytokine release syndrome (CRS) and neurotoxicity, which can be lethal [11].

To overcome these challenges, we chose to exploit the natural ability of NK cells to directly kill target cells and simultaneously trigger an adaptive immune response. Previous studies showed that CAR-NK cells were able to effectively kill CD19⁺ leukemic cells [12]. Furthermore, NK cells harbor a high potential for an off-the-shelf product, based on the lack of need for HLA matching and use of allogenic sources without severe adverse effects [13]. Additionally, irradiated NK-92 cells can be administered in high doses to patients and have shown strong safety track records [14]. The possibility to use NK-92 cell lines for clinical applications greatly decreases the costs for off-the-shelf CAR treatments, which supports further CAR-NK-92 cell research. Here, we investigated CAR-NK-92 cells designed to target HER1, which is overexpressed in over 80% of HNSCC [15]. Furthermore, HER1 expression is responsible for tumor proliferation, formation of metastasis and treatment resistance, and hence associated with poor prognosis, making it a compelling target antigen [16].

In the present study, we compared cytotoxicity of six anti-HER1 CAR-NK-92 cell variants, generated primary HNSCC (pHNSCC) cell lines and demonstrated effective elim-

ination of pHNSCC cells as well as SCC cell lines by our anti-HER1 CAR-NK-92 cells in 2D and 3D models. Anti-HER1 CAR-NK-92 cells also displayed increased apoptosis induction, CD107a expression and IFN γ secretion in co-culture with target cells, emphasizing the promising potential of CAR-NK cell therapy in HNSCC.

2. Materials and Methods

2.1. Cell Culture and Cell Lines

SCC-4 and SCC-25 cell lines (DSMZ, Braunschweig, Germany) were cultivated in DMEM/F12 GlutaMax medium (Thermo Fisher Scientific, Waltham, MA, USA) supplemented with 10% fetal bovine serum (FBS Standard, PAN-Biotec, Aidenbach, Germany) and 1% penicillin/streptomycin (P/S; PAN-Biotec). NK-92 cells (DSMZ) were cultivated in RPMI 1640 medium (PAN-Biotec) supplemented with 10% FBS, 1% P/S, 1 mM sodium pyruvate (PAN-Biotec) and 400 U/mL human IL2 (PeproTech, Winterhude, Germany). All cells were cultured under standard humidified conditions at 37 °C and 5% CO₂.

2.2. Isolation and MACS-Sorting of Primary HNSCC Cells

Primary HNSCC (pHNSCC) tumor samples were obtained from the Department of Otolaryngology at Hannover Medical School following patient informed consent according to the Declaration of Helsinki and following approval from the local ethics committee (No. 9573_BO_K2021). pHNSCC tumor pieces were digested in 1 × HBSS (GIBCO, Life Technologies, Carlsbad, CA, USA) containing 3 mg hyaluronidase (Sigma–Aldrich, St. Louis, MO, USA) and 10 mg collagenase II (StemCell Technologies, Vancouver, BC, Canada). Erythrocytes were lysed using lysis buffer (BD Biosciences, Franklin Lakes, NJ, USA). Isolated pHNSCC were immediately stored at –180 °C, analyzed or MACS sorted. pHNSCC were MACS-sorted for EpCAM according to the manufacturer’s instructions (Miltenyi Biotec, Bergisch Gladbach, Germany). Sorted cells were cultured in PneumaCult Ex medium (StemCell Technologies) supplemented with 50× supplement and 1% P/S at 37 °C and 5% CO₂.

2.3. Generation of Retroviral Vectors and Viral Supernatant Production

Third generation CARs carrying CD28, 41BB and CD3 ζ domains were cloned into self-inactivating alpharetroviral backbones carrying an IRES-eGFP cassette for easy detection [17]. Three different anti-HER1 single-chain variable-fragments (scFv) derived from different patents were used: **7D6**, **12D3** (WO 2Ull/156ol7 A2) and **2F8** (WO 02/100348 A2). Alpharetroviral vectors were pseudotyped with RD114TR, while lentiviral vectors were pseudotyped with VSVg. All viral vector supernatants were generated using HEK-293T cells (DSMZ) and calcium-phosphate transfection with split packaging design (alpharetroviral vector production: 5 μ g alpharetroviral vector construct, 2.5 μ g pcDNA3- α -gag/pol.co and 2 μ g pHCMV-RD114TR; lentiviral vector production: 5 μ g lentiviral vector construct, 12 μ g pcDNA3.GP.4xCTE, 6 μ g pRSV-Rev and 2 μ g pMD.G-VSVg).

2.4. Transduction of Cell Lines with Retroviral Vectors

Transduction was done on retronectin (Takara Bio, Otsu, Japan) coated 48-well plates. Wells were loaded with viral supernatant and centrifuged (400 × g, 4 °C, 30 min). Next, 1 × 10⁵ NK-92 cells were seeded per well. For transduction with the lentiviral vector, 1 × 10⁵ SCC or pHNSCC cells were seeded on a 24-well plate. Next, viral supernatant was added in medium containing protamine sulfate. Transduced NK-92 cells and all target cells were sorted at the cell sorting core facility at Hannover Medical School.

2.5. Bradford Assay and Western Blotting

Total protein concentrations of cell lysates were determined with the Coomassie dye-binding assay (Bio-Rad Laboratories, Hercules, CA, USA). For Western blot analysis, membranes were incubated with anti-CD3 ζ -HRP (1:1000, Santa Cruz Biotechnology, CA,

USA) in 5% milk. After detection, membranes were stripped and reprobed with anti-GAPDH-HRP (1:10,000, GeneTex/BIOZOL, Eching, Germany) in 5% milk.

2.6. gDNA Isolation and Vector Copy Number Determination

To determine vector copy number, gDNA was isolated using the QIAamp DNA blood Mini Kit (QIAGEN, Hilden, Germany) and amplified using Taqman qPCR technology using Taqman Fast Advanced Master Mix according to manufactures instruction (Thermo Fisher Scientific). (Sequences: *WPRE* forward GAGGAGTTGTGGCCCCGTTGT; *WPRE* reverse TGACAGGTGGTGGCAATGCC; *WPRE* probe CTGTGTTTGTGACGCAAC; *PTBP2* forward TCTCCATTCCTATGTTTCATGC; *PTBP2* reverse GTTCCCAGCAATGGTGAGGTG; *PTBP2* probe ATGTTCTCGGACCAACTTG).

2.7. Optical Genome Mapping

Optical Genome Mapping (OGM) was performed according to the manufacturer's instructions. Briefly, DNA was isolated from 1.5×10^6 frozen cells using the Bionano Prep SP Frozen Cell Pellet DNA Isolation Protocol v2 (#30398 Rev B, Bionano Genomics Inc., San Diego, CA, USA). The DNA concentration was determined with the QubitTM dsDNA BR Assay Kit and a Qubit 3.0 Fluorometer (Thermo Fisher Scientific). Subsequently, the DNA was labeled with Bionano Prep Direct Label and Stain Kit (Protocol #30206 Rev G; Bionano Genomics Inc.) and the concentration determined with the QubitTM dsDNA HS Assay Kit and a Qubit 3.0 Fluorometer (Thermo Fisher Scientific). The labeled DNA was loaded on a Saphyr G2.3 chip and imaged with the Saphyr device (Bionano Genomics Inc.). The data were analyzed and visualized on the Bionano Access Server with the de novo pipeline (Tools Version 1.7.1, reference genome GRCh38/hg38). The recommended filter settings were applied and the frequency of SVs in the Bionano control database was set to 0%.

2.8. Flow Cytometry: Cytotoxicity Assay

For detection, target cells were stained with 1 μ M FarRed CellTrace according to manufacturer's instruction (Thermo Fisher Scientific) and then seeded in RPMI medium on one 48-well plate/per time point (0, 24, 48 h). The next day, unmodified and CAR-NK-92 cells were seeded on top in specific effector:target cell (E:T) ratios. For each time point, co-cultures were stained with anti-HER1 BV605 (BioLegend, San Diego, CA, USA) and/or anti-CD44v6 PE (R&D Systems, Minneapolis, MN, USA) and analyzed with a CytoFLEX S flow cytometer (Beckman Coulter, Brea, CA, USA) to acquire events in 80 μ L. Cytotoxicity was calculated as shown below, whereby the proliferation rate of target and effector cells was factored in.

$$\text{remaining target cells} = \frac{\text{target cells}}{(\text{target cells} + \text{effector cells})} * 100$$

2.9. Automated Live-Cell Imaging: Cytotoxicity Assay and 3D Spheroid Assay

For cytotoxicity assays, $0.35\text{--}1.2 \times 10^4$ mCherry⁺ target cells were seeded on 96-well plates. The next day, CAR-NK-92 cells were seeded in complete RPMI medium containing IL-2, 1 mM CaCl₂ and Annexin V NIR dye (Sartorius, Göttingen, Germany). For spheroid formation, $0.35\text{--}1.5 \times 10^4$ mCherry⁺ SCC-4, SCC-25 or primary HNSCC cells were seeded on ultra-low attachment 96-well plates (S-BIO, Singapore, Central Region, Singapore). After 72 h, CAR-NK-92 cells were seeded on top. Plates were analyzed using Incucyte SX5 Live-Cell Analysis instrument (Sartorius).

2.10. CD107a Degranulation Assay

NK-92 cells were starved of IL-2 for 24 h before and throughout the duration of the experiment. The next day, NK-92 cells were seeded together with target cells using an E:T ratio of 1:1 in complete RPMI medium. Co-cultures were incubated with monensin, Brefeldin A and anti-CD107a antibody (Miltenyi Biotec) and cultivated for 4 h total. Next, cells were incubated with anti-Flag PE (BioLegend, San Diego, CA, USA) and anti-CD56

PC7 (BD Biosciences, Franklin Lakes, NJ, USA). Afterwards, the cells were fixed with fixation buffer (BioLegend) and analyzed using a CytoFLEX S (Beckman Coulter).

2.11. IFN γ Secretion

NK-92 cells were starved of human IL-2 for 24 h prior to seeding and during the co-culture experiment (except for the screening of six anti-HER1 CAR-NK-92 cells, which was conducted with human IL-2). IFN γ secretion was analyzed using human IFN γ ELISA according to the manufacturer's instructions (BioLegend). Briefly, the IFN γ standards provided by the ELISA kit were used as positive controls (7.8, 15.6, 31.3, 62.5, 125, 250 and 500 pg/mL) and 1X Assay Diluent A was used as the zero standard (0 pg/mL) or negative control. Dilutions of the IFN γ standard were used to quantify IFN γ released from the NK-92 cells according to the manufacturer's instructions.

2.12. Immunohistochemistry Staining and Analysis

Immunohistochemical staining was performed on paraffin sections (2 μ m thickness). All sections were deparaffinized with xylene twice, rehydrated using decreasing ethanol concentrations, and then subjected to heat-induced epitope retrieval in antibody buffer. Stainings were performed using the antibodies listed in Supplementary Table S1, the ZytoChem Plus HRP Polymer Kit (Zytomed Systems, Berlin, Germany), 3,3'-diaminobenzidine solution (DAB), hematoxylin counterstain and the Eukitt mounting medium. Stained slides were digitized using the Nano Zoomer S210 (Hamamatsu Photonics, Herrsching a. Ammersee, Germany). DAB-positive and negative cells were counted with the nuclei detection image analysis application of Visiopharm (Visiopharm, Hørsholm, Denmark).

2.13. Statistical Analysis

Statistical analysis was performed via GraphPad Prism 6.01 software (GraphPad Software, San Diego, CA, USA) and two-way ANOVA with Bonferroni's post-hoc test. * indicates comparison to unmodified NK-92 cells within time points (e.g., 24 h to 24 h) unless specified otherwise. Error bars in all figures depict the standard deviation of the mean. * = $p < 0.05$, ** = $p < 0.01$, *** = $p < 0.001$, **** = $p < 0.0001$.

3. Results

3.1. Validation of Anti-HER1 CAR Expression in NK-92 Cells

Six CAR-NK variants were created using single-chain variable fragments (scFv) 7D6, 12D3, 2F8, and each of which was combined with a long (CH2CH3) and a medium (CH3) hinge version (Figure 1A). Transduction efficiency was assessed using eGFP expression six days post-transduction (Figure 1B). To generate high-purity CAR-NK-92 cells, cells were sorted for flag-APC⁺eGFP⁺ expression and demonstrated >88% flag-tag, hence CAR surface expression, three weeks after sorting (Figure 1C). Western blot analysis was used to validate full-length CAR-CD3 ζ protein expression, which varied in size (60 or 80 kDa) depending on the IgG1-based hinge type used (long hinge: CH2CH3 vs medium hinge: CH3). The 12D3 CH3 CAR variant showed an additional protein band at 40 kDa, which may be a degradation product. Unmodified and eGFP-transduced NK-92 cells serve as controls, which lack CAR-based CD3 ζ expression and only showed endogenous CD3 ζ expression at 15–18 kDa, which was also apparent for all transduced CAR variants (Figure 1D). Determination of vector copy number (VCN) quantifies the *wPRE* sequence of the alpharetroviral vector backbone in relation to *PTBP2* as a housekeeping control. Similar vector integrations levels were achieved in all CAR-NK-92 cells. eGFP-NK-92 control cells (no CAR) showed VCN of 7.41, indicating a better transduction efficiency, possibly due to the smaller vector size (Figure 1E). CAR-NK-92 cells were monitored for flag-tag expression via flow cytometry over several weeks after sorting and a loss of CAR expression was observed for variants 7D6 CH3 (<60%) and 2F8 CH2CH3 (<20%) after 15–20 weeks. All remaining variants

maintained a stable CAR expression as indicated by the expression of the flag-tag in more than 80% of cells over several weeks (Figure 1F).

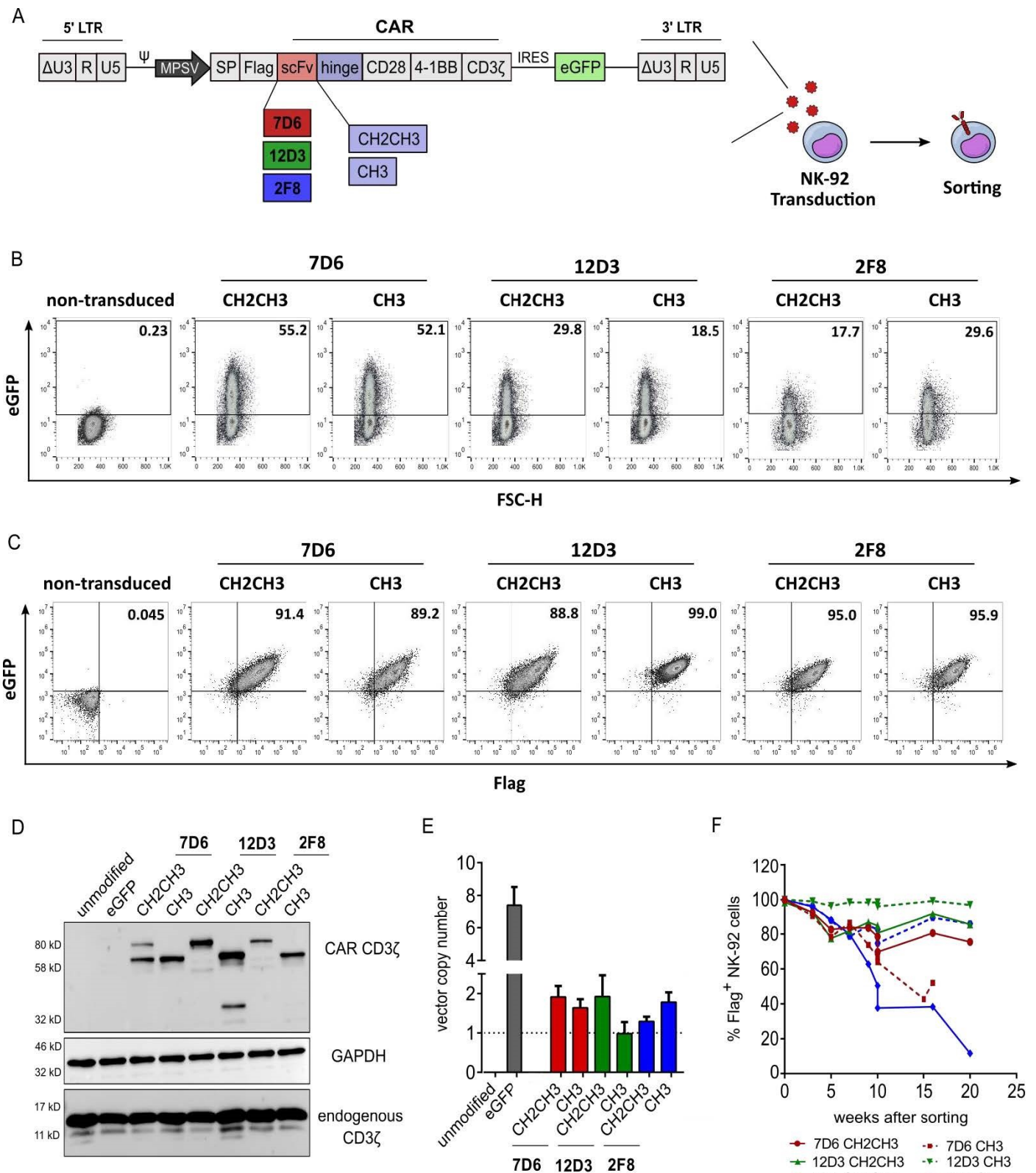


Figure 1. Transduction and expression of six anti-HER1 CAR-NK-92 candidates. (A) Vector design showing self-inactivating alpharetroviral backbones, third generation CAR and an IRES-eGFP cassette.

Three anti-HER1 single chain variable fragments (scFv) 7D6, 12D3 and 2F8 were each combined with long (CH2CH3) and medium (CH3) hinges to generate six anti-HER1 CAR-NK-92 candidates. (B) Transduction efficiency was assessed by percentage of eGFP⁺ expression via flow cytometry. (C) CAR expression 3-weeks post sorting for flag-APC⁺ eGFP⁺ cells. Analysis of CAR expression and vector integration via (D) Western blot (CAR CD3 ζ = 60 or 80 kDa, GAPDH = 37–38 kDa, endogenous CD3 ζ = 15–18 kDa), see the Supplementary File S1 for the original images of Western blot. (E) vector copy number analysis and (F) flow cytometry. Mean with standard deviation shown, n = 3.

3.2. Functional Screening of Six Anti-HER1 CAR-NK-92 Cell Variants

Prior to assessing cytotoxic functionality, we characterized two HNSCC cell lines SCC-4 and SCC-25 using Optical Genome Mapping (OGM). Both cell lines clearly depicted the genetic heterogeneity of this cancer as evidenced by the different types of genetic aberrations, including aneuploidies, translocations, duplications and deletions. While SCC-4 cells (Figure 2A) showed a more complex profile of genetic aberrations compared to SCC-25 cells (Figure 2B), some similarities were detected, including high-fold amplification on chromosome 11q13 (Figure 2, Supplementary Figure S1). This region harbors genes associated with tumor progression and cell cycle control, including cyclin D1/PRAD1 and BCL-1 [18]. To ensure recognition by the various anti-HER1 CAR-NK-92 cells, SCC-4 and SCC-25 cells were examined for HER1 expression and found to be highly positive (>99%) (Supplementary Figure S1). For the functional screening, the genetically more complex cell line SCC-4 was used as a target cell line. Here, SCC-4 cells were harvested, stained with FarRed CellTrace and seeded on day 0. The next day, co-cultures of all six anti-HER1 CAR-NK-92 variants were seeded using different E:T ratios. Cells were harvested at 0, 24 and 48 h after initiation of co-culture, stained for HER1 and analyzed using flow cytometry (Figure 2C). At 5:1 and 10:1 E:T ratios, improved killing effects were observed for all CAR variants after 24 h and 48 h, except for 2F8 CH2CH3 CAR-NK-92 cells. This can be explained by loss of CAR expression seen in Figure 1, as the functionality was assessed around a similar time as the loss of CAR expression was observed. No CAR construct appeared superior to the others regarding killing activity throughout 24 h and 48 h and different E:T ratios (Figure 2D). Furthermore, proliferation rates of 2-3-fold of transduced NK-92 cells were comparable in co-culture compared to unmodified NK-92 cells after 48 h. SCC-4 cells alone also proliferated well, despite the medium change to RPMI with up to 2-fold within 48 h (Figure 2E). As an additional functional readout, IFN γ secretion after 48 h co-culture was assessed via ELISA. Unmodified and eGFP-NK-92 cells showed no increased IFN γ secretion upon co-culture with SCC-4 cells, while all CAR-NK-92 cells showed increased IFN γ secretion in the presence of SCC-4 cells (Figure 2F, IFN γ ELISA of E:T ratios 1:1 and 10:1 found in Supplementary Figure S2).

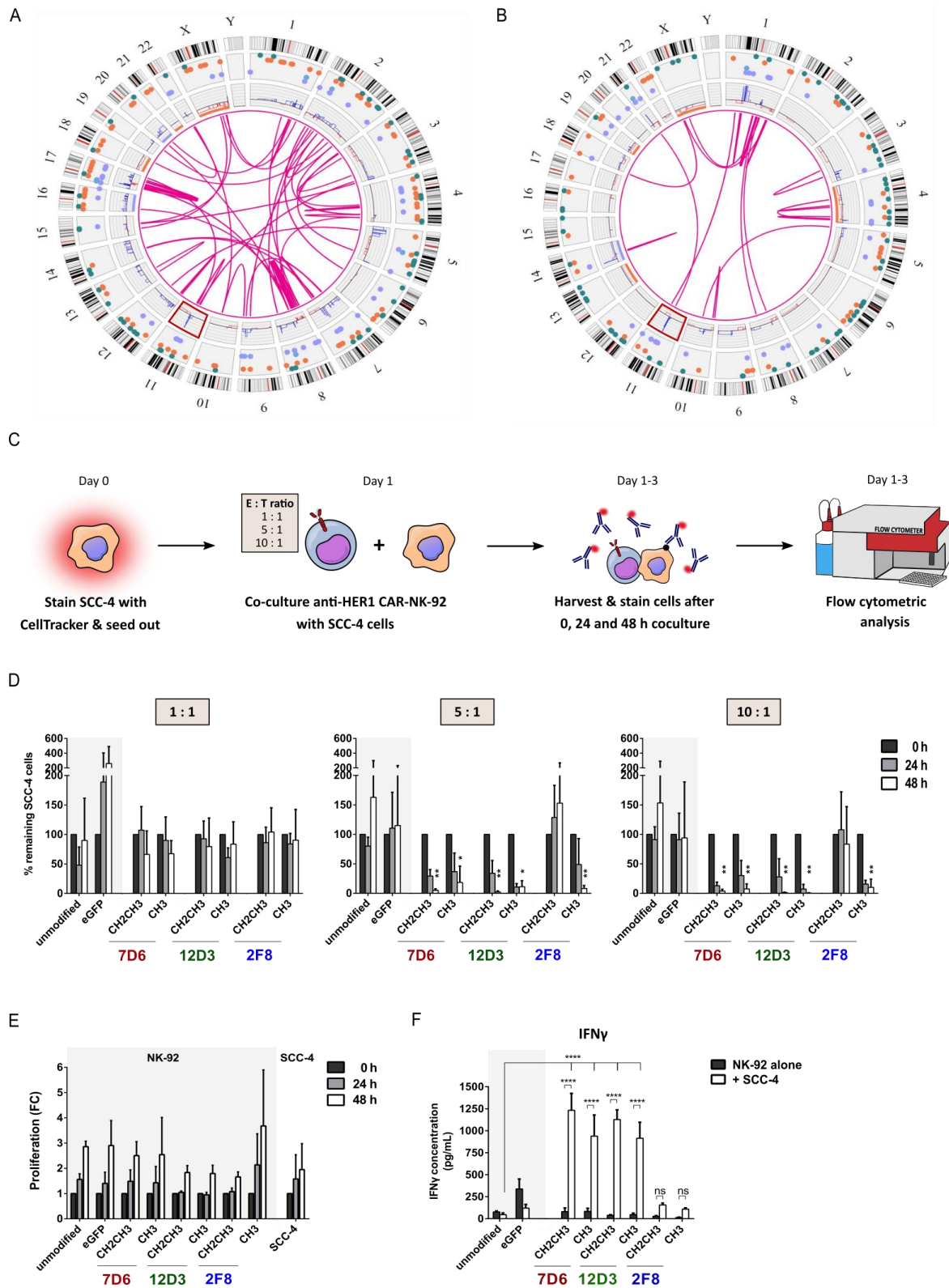


Figure 2. Functional screening of six anti-HER1 CAR-NK-92 cell candidates. Characterization of SCC-4 cells (A) and SCC-25 cells (B) using OGM. Red box highlights amplification at 11q13 (Legend: ● copy number gains (blue lines), ● copy number losses (red lines), ● insertions, ● deletions, ● inversions, ● duplications, ● intra-fusions or inter-translocations (pink lines)). (C) Experimental design of flow cytometry-based cytotoxicity assay. (D) Cytotoxicity assay using anti-HER1 CAR-NK-92 candidates and SCC-4 cells. (E) Proliferation of CAR-NK-92 cells in co-cultures and SCC-4 cell monocultures

during cytotoxicity assay. (F) IFN γ ELISA using supernatant from 48 h time point of cytotoxicity assay (5:1 E:T ratio). E:T = effector:target cell ratio. Mean with standard deviation shown. Statistical analysis was performed using two-way ANOVA with Bonferroni's post-hoc test for comparison to unmodified NK-92 cells within the same time points (e.g., 24 h to 24 h), $n = 3$. * = $p < 0.05$, ** = $p < 0.01$, **** = $p < 0.0001$.

3.3. Anti-HER1 CAR-NK-92 Variants Showed Enhanced Killing, Apoptosis Induction and Degranulation against SCC-4 and SCC-25 Cell Lines

Based on stable long-term CAR expression, lack of tonic signaling (Supplementary Figure S3) and HNSCC killing activity, anti-HER1 CAR-NK-92 cell variants 12D3 CH3 and 2F8 CH3 were selected as the most promising candidates and used for all further experiments. For more suitable controls, internally truncated versions of these two CARs that lack signaling and effector domains (Δ CAR) and one externally truncated CAR (ex Δ CAR), that lacks the extracellular scFv and hinge domains were generated and used to transduce NK-92 cells. Flow cytometry-based cytotoxicity assays showed enhanced killing of SCC-4 cells only upon co-culture with full-length 12D3 CH3 and 2F8 CH3 CAR-NK-92 cells after 24 h and 48 h using 5:1 E:T ratios (Figure 3A). This was confirmed using an Incucyte-based cytotoxicity assay, which showed that the strongest killing effect of 12D3 CH3 and 2F8 CH3 CAR-NK-92 cells occurred within 10 h of co-culture initiation. Monocultures of SCC-4 cells continued to proliferate, while co-culture with unmodified NK-92 cells and ex Δ CAR-modified NK-92 cells prevented SCC-4 proliferation, further confirming the flow cytometry-based results. Additionally, Annexin V staining showed enhanced apoptosis rate in co-cultures with both full length CAR-NK-92 cell variants within 10 h of co-culture initiation, which reflected the rapid decline of SCC-4 cells in these co-cultures (Figure 3B). The nearly complete loss of SCC-4 cells upon co-culture with NK-92 cells modified with full-length CARs was also evident in microscopy pictures at 12 h, which indicated clustering of eGFP⁺ CAR-NK-92 cells around the few remaining mCherry⁺ SCC-4 cells compared to co-cultures with unmodified or ex Δ CAR-modified NK-92 cells (Figure 3C). SCC-25 cells were already effectively killed at an E:T ratio of 0.5:1 using 12D3 CH3 and 2F8 CH3 CAR-NK-92 cells after 24 h and 48 h compared to the controls in the flow cytometry-based cytotoxicity assay (Figure 3D). Similar results were obtained with the Incucyte-based cytotoxicity assay. Furthermore, the rate of apoptosis in co-cultures of SCC-25 cells with full-length CAR-NK-92 cells was greatly enhanced within 10 h compared to unmodified and ex Δ CAR-NK-92 control cells, which concurs with data from SCC-4 cells (Figure 3E). During the automated live-cell imaging, the same phenomenon of strong reduction of mCherry⁺ SCC-25 cells was apparent after 12 h in co-cultures with NK-92 cells modified with full-length 12D3 CH3 and 2F8 CH3 CARs. Moreover, greater clustering around SCC-25 cells and higher rates of apoptosis were visible upon co-culture with full-length CAR-NK-92 cells compared to untreated SCC-25 cells or co-cultures with unmodified or ex Δ CAR-NK-92 cells (Figure 3F). As an additional indication of targeted NK-92 cell activity, elevated IFN γ levels were only observed in ELISA analysis after co-culture of SCC-4 or SCC-25 cells with 12D3 CH3 and 2F8 CH3 CAR-NK-92 cells (Figure 3G). The IFN γ secretion of CAR-NK-92 cells in monocultures remained at the same level as unmodified NK-92 cells. To determine the mechanism of cytotoxic killing, we examined expression of degranulation marker CD107a on NK-92 cells after 4 h co-culture with SCC-4 and SCC-25 cells. Monocultures of 12D3 CH3 CAR-NK-92 cells showed a 2-fold upregulation of CD107a MFI compared to unmodified NK-92 cells alone. Moreover, 12D3 CH3 CAR-NK-92 cells also showed an upregulation of CD107a MFI by 5-fold in the presence of SCC-4 cells and by 4-fold in the presence of SCC-25 cells (Figure 3H). 2F8 CAR-NK-92 cells showed no enhanced expression of CD107a, which suggests that target cell killing is likely to occur via another mechanism. A possible mechanism could be induction of death receptor-mediated apoptosis via upregulated expression of TRAIL or FAS ligands; however, this was not assessed in this study.

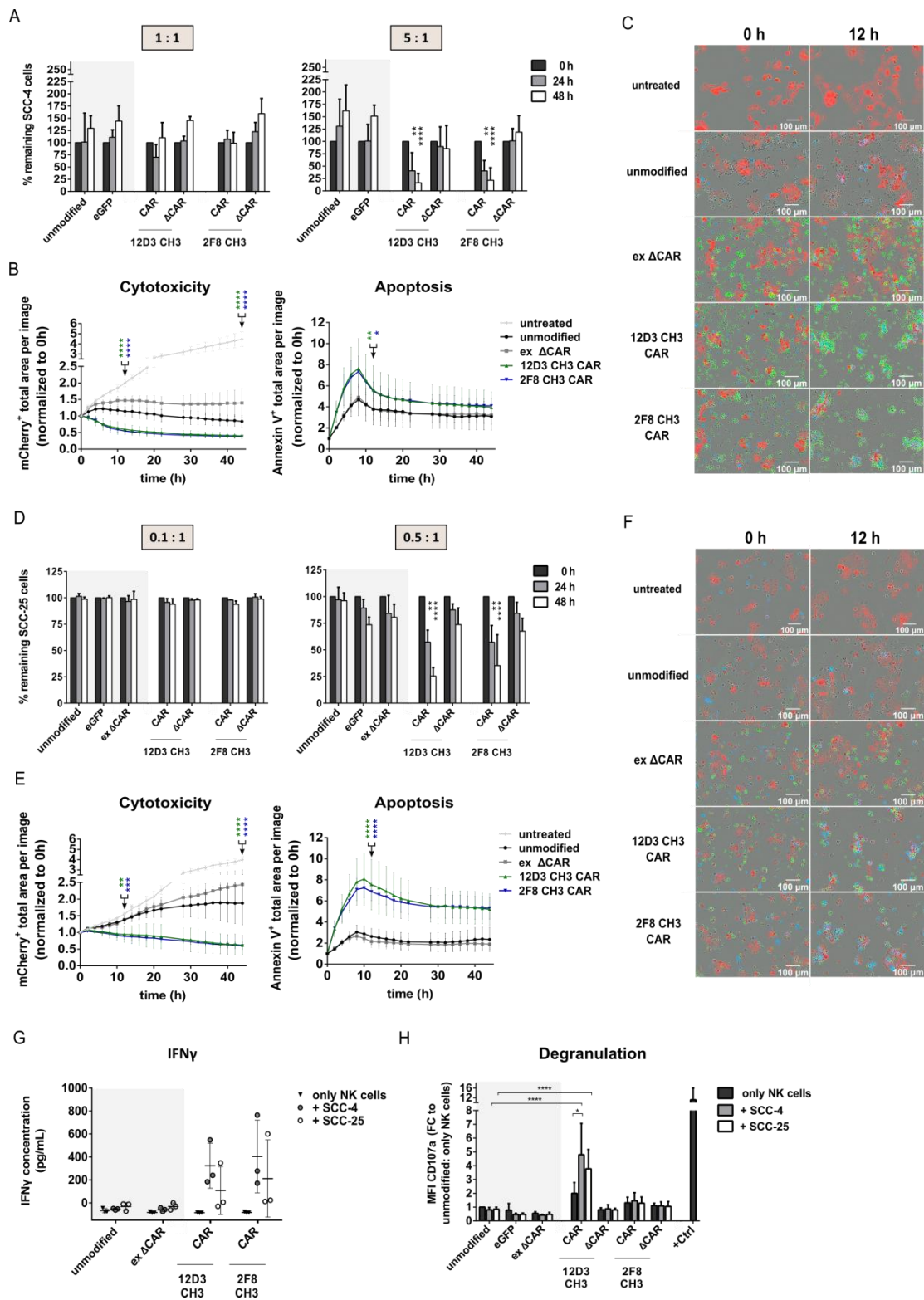


Figure 3. Enhanced cytotoxic capacity, apoptosis induction, IFN γ secretion and degranulation of 12D3 CH3 and 2F8 CH3 CAR-NK-92 cells. (A) Flow cytometry-based and (B) Incucyte-based cytotoxicity assays against SCC-4 cells. (C) Automated live-cell imaging using Incucyte against SCC-4 cells (red: mCherry⁺ SCC-4 cells; green: eGFP⁺ CAR NK-92 cells; blue: Annexin V⁺ cells). (D) Flow cytometry-based and (E) Incucyte-based cytotoxicity assay against SCC-25 cells. (F) Automated live-cell imaging using Incucyte against SCC-25 cells (red: mCherry⁺ SCC-25 cells; green: eGFP⁺ CAR NK-92 cells; blue: Annexin V⁺ cells). (G) IFN γ ELISA of 48 h supernatant from co-cultures with SCC-4 cells (5:1 E:T ratio)

and with SCC-25 cells (0.5:1 E:T ratio). (H) CD107a expression of NK-92 cells after 4 h co-culture of 1:1 E:T ratio for both target cell lines. +Ctrl consists of PMA/Ionomycin stimulated NK-92 cells. E:T = effector:target cell ratio; FC = fold change. Mean with standard deviation shown. Statistical analysis was performed using two-way ANOVA with Bonferroni's post-hoc test for comparison (A,D) to unmodified NK-92 cells within time points (e.g., 24 h to 24 h) or (B,E) between full-length CAR-NK-92 cells and unmodified NK-92 cells at 12 h and 44 h. $n = 3$, except for Incucyte data $n = 9$ (Incucyte experiments and ELISA were performed with three separate transduction rounds of NK-92 cells). * = $p < 0.05$, ** = $p < 0.01$, *** = $p < 0.001$, **** = $p < 0.0001$.

3.4. Isolation and Characterization of Primary HNSCC Tumor-Derived Cells

To examine effectivity of selected anti-HER1 CAR-NK-92 cells against primary HNSCC (pHNSCC)-derived cells, we isolated and characterized pHNSCC cells (Table 1). Most patient samples were HPV⁻ and of primary occurrence, without treatment at the time of biopsy. To determine the isolated cell types, we assessed expression of hematological markers, stroma, endothelial, cancer-associated fibroblast and epithelial markers. CD45 expression varied highly between patient samples from 21.6% to over 87.5% CD45⁺ cells, suggesting a high presence of immune cells within the tumors (Figure 4A). The CD45⁺ cell population largely consisted of T cells and macrophages, but also contained NK cells, B cells and other cells (Figure 4B). The CD45⁻ population was screened for endothelial cells and stroma cells, which were only present at low percentages (<30%). As EpCAM expression was shown to be highly specific in carcinomas, especially HNSCC [19], we used the epithelial marker EpCAM to characterize the largely unknown cell population in patient samples #1, #2, #3 and #13. Approximately 60–70% of CD45⁻ cells in freshly isolated patient samples were EpCAM⁺, with the exception of sample #6 (Figure 4C). After confirming that SCC-4 and SCC-25 cell lines are also entirely EpCAM⁺ (Supplementary Figure S4), we used a previously published EpCAM⁺ cell sorting approach to establish pHNSCC cell cultures, and used PneumaCult Ex medium (StemCell Technologies, Vancouver, BC, Canada) for improved epithelial growth [20]. However, to get an unbiased idea of target antigen expression, we assessed surface marker expression on freshly isolated pHNSCC samples before sorting. Despite strong variation among samples, HER1 expression was highest, followed by CD44v6, while CD133 was expressed at low very low levels, suggesting HER1 as a promising target antigen (Figure 4D). This was also consistent with immunohistochemical (IHC) staining, which also demonstrated co-localization of HER1⁺ and CD44v6⁺ cells (Supplementary Figures S6 and S7) and stronger HER1 expression than CD44v6. Furthermore, IHC staining also supported a greater presence of CD3⁺ T cells and CD11b⁺ macrophages than CD56⁺ NK cells and CD19⁺ B cells (Figure 4E, Supplementary Figures S6 and S7). Next, we ensured HER1 expression persisted throughout the sorting procedure. HER1 expression exceeded 50% on four out of five patient samples (Figure 4F). Furthermore, HER1 expression on cells from patient sample #7 increased throughout the sorting process from 11.7% to 51.8%, which can be explained by the loss of non-epithelial cells. Expanded EpCAM-sorted pHNSCC samples #14 and #16 were also used for OGM (Figure 4G,H, respectively). Although fewer overall genetic aberrations were observed in the pHNSCC samples as compared to SCC-4 and SCC-25 cell lines, it may be of interest that both patient samples analyzed exhibited the same chromosome 11q13 amplification that was identified in the SCC-4 and SCC-25 cell lines (Figure 4G,H, Supplementary Figure S4).

Table 1. Primary HNSCC patient samples analyzed.

Sample	Region	HPV Status	Tumor Occurrence	Treatment Post Biopsy
#1	Tongue	negative	primary	primary RCTx
#2	Tonsil right	negative	primary	primary RCTx
#3	Parapharyngeal	/	primary	primary RCTx
#4	Nose skin	negative	primary	surgery, no RCTx
#5	Tonsil left	positive	primary	surgery, no RCTx

Table 1. Cont.

Sample	Region	HPV Status	Tumor Occurrence	Treatment Post Biopsy
#6	Soft palate	negative	primary	primary RCTx
#7	Oropharynx right	negative	primary	primary RCTx
#8	Larynx	/	primary	/
#9	Tongue basis	positive	primary	primary RCTx
#10	Hypolarynx	negative	primary	primary RCTx
#11	Larynx	negative	secondary	surgery, no RCTx
#12	Uvula	positive	primary	none
#13	Uvula	negative	primary	primary RCTx
#14	Tonsils	negative	primary	primary RCTx
#15	Tonsil	negative	primary	primary RCTx
#16	Tongue	negative	secondary	Surgery, no RCTx

RCTx = radio- and chemotherapy, / = no information available.

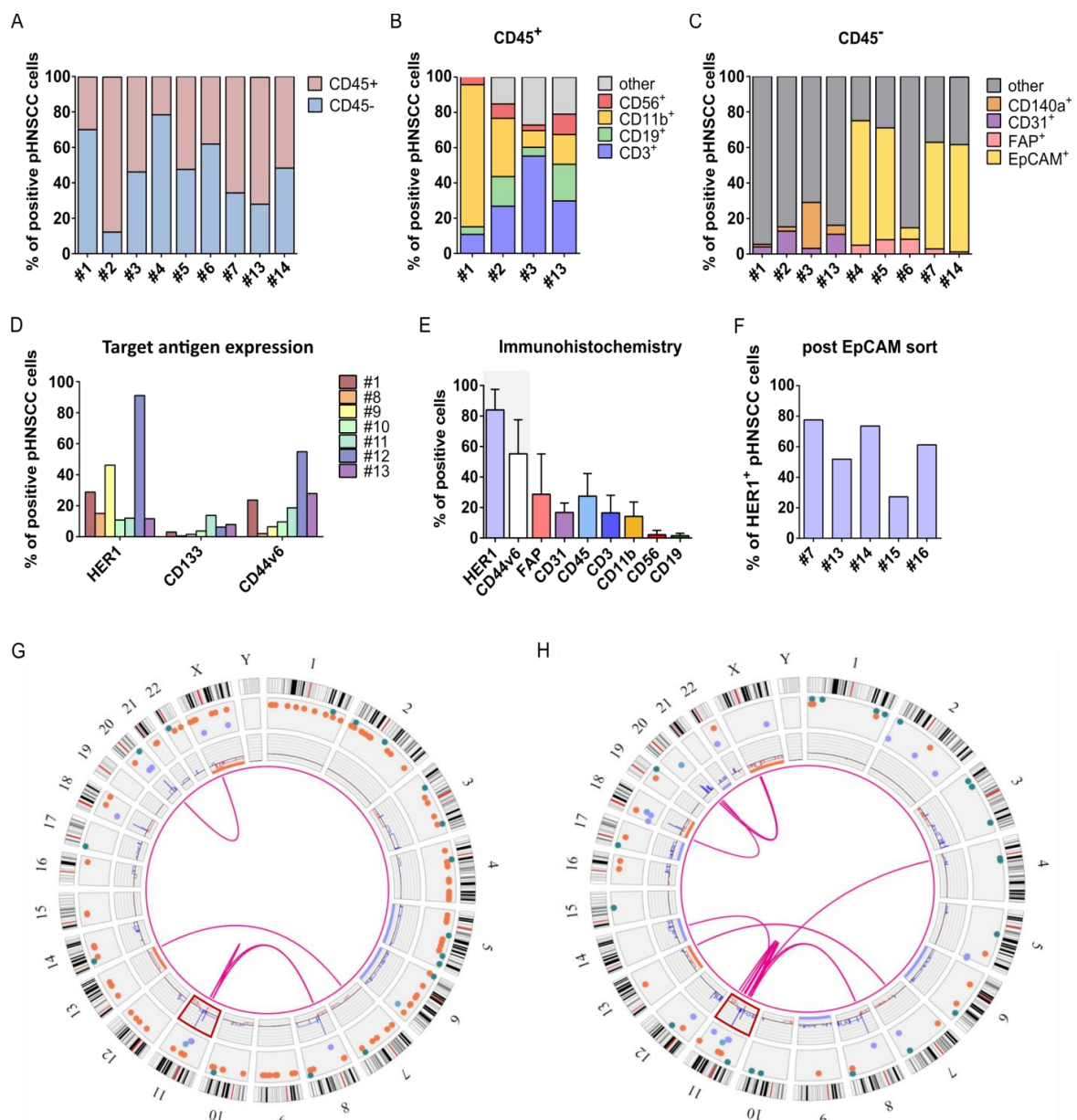


Figure 4. Characterization of primary HNSCC (pHNSCC) cells. Characterization of (A) CD45+ immune cells present in isolated pHNSCC samples as well as (B) percentage of NK cells (CD56+),

macrophages (CD11b⁺), B cells (CD19⁺) and T cells (CD3⁺) of CD45⁺ cells in pHNSSC samples and (C) percentages of stroma cells (CD140a⁺), endothelial cells (CD31⁺), cancer-associated fibroblasts (FAP⁺) and epithelial marker-positive cells (EpCAM⁺) in the CD45⁺ pHNSSC cell population within 24 h from isolation (or thawing). (D) Target antigen expression within 24 h of isolation (or thawing) of pHNSSC samples. (E) Quantitative analysis of immunohistochemical stainings of seven patient samples (photos from exemplary patient samples shown in Supplementary Figures S6 and S7). (F) HER1 expression on EpCAM⁺ sorted and expanded pHNSSC samples. Optical genome mapping of EpCAM⁺ sorted and expanded pHNSSC samples (G) #14 and (H) #16. Red box highlights amplification of 11q13, (Legend: ● copy number gains (blue lines), ● copy number losses (red lines), ● insertions, ● deletions, ● inversions, ● duplications, ● intra-fusions or inter-translocations (pink lines)). Mean with standard deviation shown. n = 4–9 pHNSSC samples as indicated (A–E).

3.5. Anti-HER1 CAR-NK-92 Cells Show Enhanced Killing, Apoptosis and Degranulation against pHNSSC Cells

Enhanced killing of anti-HER1 CAR-NK-92 cells was validated against EpCAM⁺ pHNSSC cell lines in flow cytometry-based cytotoxicity assays using an E:T ratio of 0.5:1. Similarly to previous cytotoxicity assays, significance of killing effects was only statistically analyzed in comparison to unmodified NK-92 cells within the same time points (e.g., 24 h to 24 h). While unmodified NK-92 cells showed a strong cytotoxic killing effect against pHNSSC #13 cells after 48 h, full-length CAR-NK-92 cells had an even stronger cytotoxic effect after 24 h and 48 h. Surprisingly, eGFP-NK-92 control cells demonstrated significantly worse killing of pHNSSC #13 cells compared to unmodified NK-92 cells after 24 h and 48 h (Figure 5A, Patient #13). Unmodified, eGFP and ex ΔCAR control NK-92 cell co-cultures led to 150% of patient #14 cells after 24 h, which indicates an outgrowth of target cells compared to number of target cells seeded at 0 h (100%). This may be due to a naturally faster proliferation rate compared to other pHNSSC cell lines. After 48 h, unmodified, eGFP and ex ΔCAR control NK-92 cells were able to reduce target cells back to a similar number as at 0 h. NK-92 cells modified with 12D3 CH3 and 2F8 CH3 CARs eliminated basically all pHNSSC #14 cells after 48 h co-culture, which is consistent with the elimination of patient #13 cells (Figure 5A, Patient #14). Unexpectedly, internally truncated 12D3 CH3 control NK-92 cells also showed an improved killing effect after 48 h. A similar effect was observed for patient #16, where eGFP and both internally truncated CAR control NK-92 cells also displayed a significant killing effect compared to unmodified and ex ΔCAR control NK-92 cells. Nonetheless, NK-92 cells modified with the full-length CARs still showed significantly enhanced killing against pHNSSC cells compared to unmodified NK-92 cells after 48 h co-culture (Figure 5A, Patient #16). Simultaneously, we analyzed target antigen expression on the remaining pHNSSC cells 24 h after co-culture to ensure adequate number of events for flow cytometric analysis. For all three patient samples, the HER1⁺/CD44v6⁺ cell population decreased while CD44v6⁺ pHNSSC cells expanded surprisingly after 24 h co-cultures with full-length or internally truncated CAR-NK-92 cells compared to unmodified, eGFP and ex ΔCAR control NK-92 cells. This expansion of CSC-like cells was especially apparent in samples #13 and #16 (Figure 5B). This expansion effect of internally truncated CAR-NK-92 cells is likely due to enhanced immune synaptic formation due to the anti-HER1 scFv expressed on the NK-92 cell surface.

Incucyte analysis was performed to examine cytotoxicity and rate of apoptosis during co-culture of pHNSSC samples #14 (Figure 5C) and #16 (Figure 5D) with modified NK-92 cells. Cells from both pHNSSC patient samples were rapidly killed and showed an increased rate of apoptosis within the first 10 h of co-culture with both full-length CAR-NK-92 cells, similarly observed above for SCC-4 and SCC-25 cells. This indicates a rapid killing kinetic of the CAR-NK-92 cells against primary tumor cells even at a low E:T ratio. As previously seen in SCC-4 and SCC-25 cells, 12D3 CH3 and 2F8 CH3 CAR-NK-92 cells eliminated mCherry⁺ pHNSSC #16 cells nearly completely within 12 h. Furthermore, full-length CAR-NK-92 cells clustered around the few remaining pHNSSC #16 cells, which also displayed a visible increase in apoptotic cells as indicated by the higher Annexin V⁺ (blue)

signal within these clusters (Figure 5E). Additionally, IFN γ secretion was also significantly upregulated by 12D3 CH3 CAR-NK-92 cells to during co-culture with pHNSCC #16. For 2F8 CH3 CAR-NK-92, this effect was also apparent, but not significantly different from CAR-NK-92 cells alone (Figure 5F). The MFI of CD107a was also significantly upregulated two-to-three-fold on both full-length CAR-NK-92 cell variants upon 4 h co-culture with pHNSCC samples #14, #15 and #16 (Figure 5G) compared to unmodified NK-92 monocultures.

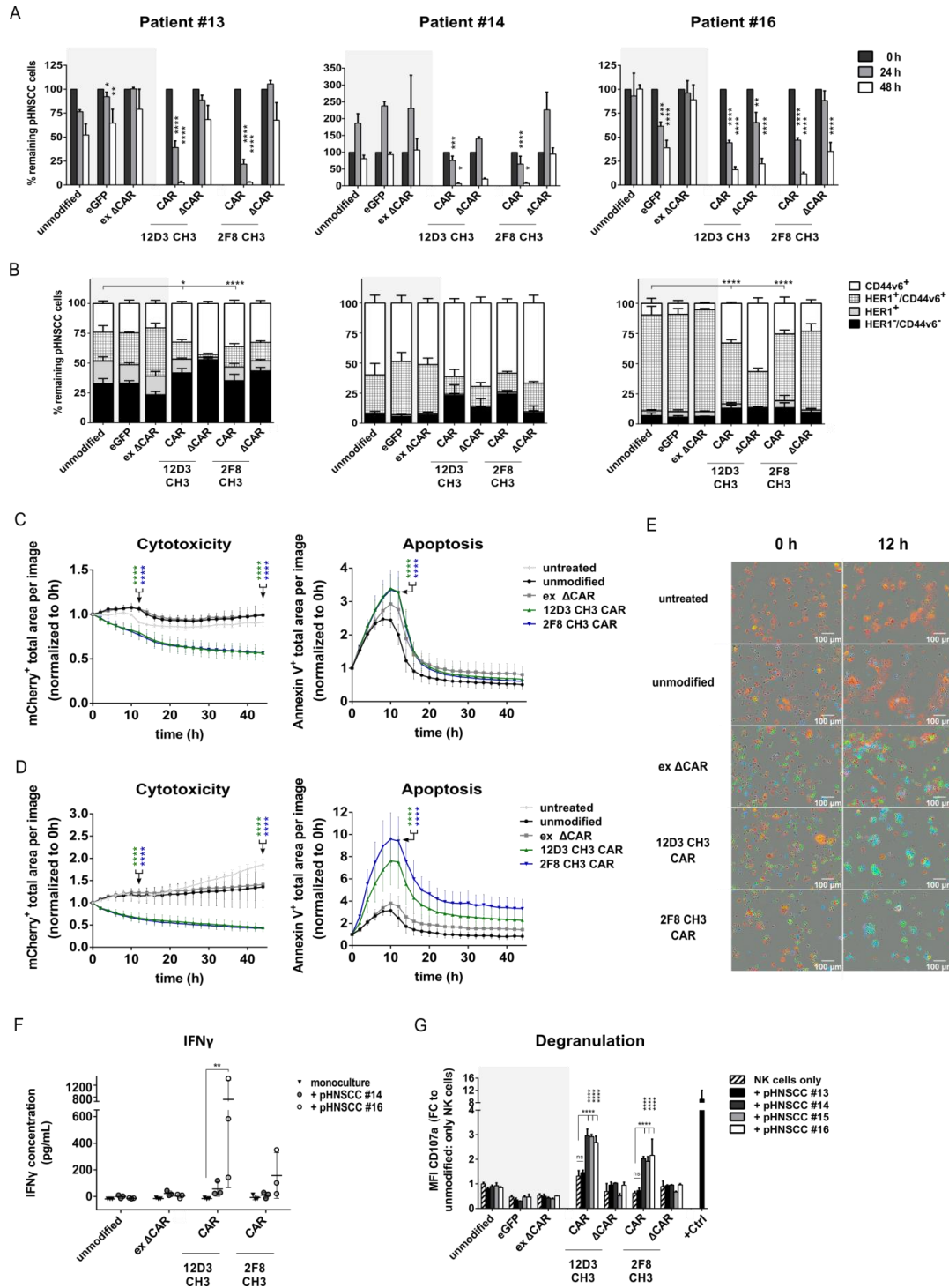


Figure 5. Anti-HER1 CAR-NK-92 cells effectively kill pHNSCC cells. (A) Flow cytometry-based cytotoxicity assay against EpCAM⁺ sorted and expanded pHNSCC samples (0.5:1 E:T ratio). (B) Target antigen expression profile of remaining pHNSCC after 24 h of co-culture with control NK-92 cells and

CAR NK-92 cells. Incucyte-based cytotoxicity assay targeting (C) pHNSCC #14 and (D) pHNSCC #16 cells (0.5:1 E:T ratio). (E) Automated live-cell imaging using Incucyte to monitor NK-92 cell activity against pHNSCC #16 cells (red: mCherry⁺ pHNSCC #16 cells; green: eGFP⁺ CAR NK-92 cells; blue: Annexin V⁺ cells). (F) IFN γ ELISA of 48 h supernatant from co-cultures (0.5:1 E:T ratio). (G) CD107a expression on NK-92 cells after 4 h co-culture at 1:1 E:T ratio for all target cell lines. +Ctrl consists of PMA/Ionomycin stimulated NK-92 cells. E:T = effector:target cell ratio; FC = fold change. Mean with standard deviation shown. Statistical analysis was performed using two-way ANOVA with Bonferroni's post-hoc test for comparison (A) to unmodified NK-92 control cells within the same time points (e.g., 24 h to 24 h), (B) between CD44v6⁺ population of full lengths CAR-NK-92 cells and unmodified NK-92 cells or (C,D) between full-length CAR-NK-92 cells and unmodified NK-92 cells at 12 h and 44 h. n = 3, except for Incucyte data n = 9 (Incucyte experiments and ELISA were performed with three separate transduction rounds of NK-92 cells). * = $p < 0.05$, ** = $p < 0.01$, *** = $p < 0.001$, **** = $p < 0.0001$.

3.6. Anti-HER1 CAR-NK-92 Treatment Resulted in Faster Spheroid Disruption

To mimic the 3D nature of tumors, we generated spheroids of mCherry⁺ SCC-4, SCC-25 and pHNSCC #16 cells, for all of which we observed a similarly rapid decline in mCherry signal intensity within 12 h of co-culture with full-length CAR-NK-92 cells compared to untreated spheroids, or co-cultures with unmodified or ex Δ CAR-NK-92 control cells, as for the 2D cultures (Figure 6A,B).

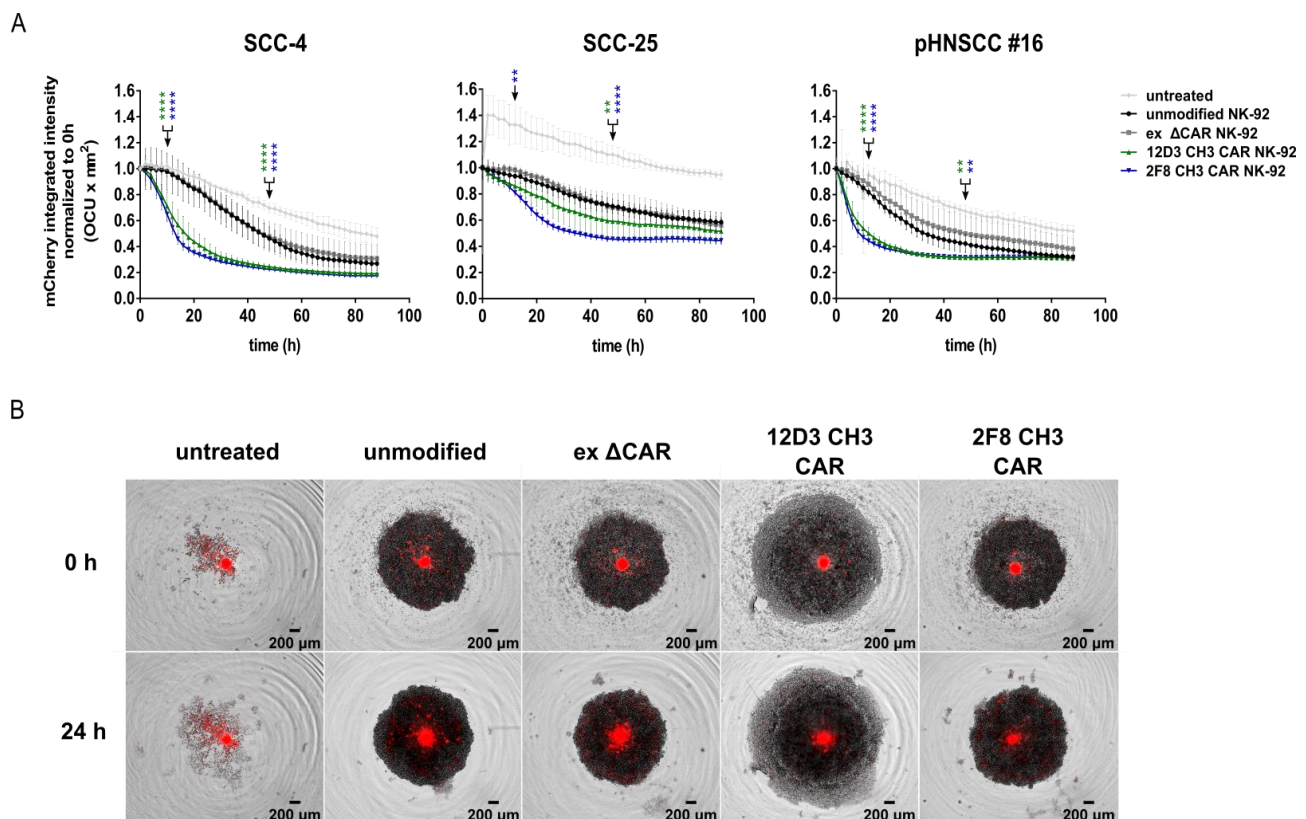


Figure 6. Efficient 3D spheroid killing upon co-culture with full-length 12D3 CH3 and 2F8 CH3 CAR-NK-92 cells. (A) Incucyte-based cytotoxicity assay using the 3D module and SCC-4 cell, SCC-25 cell and pHNSCC #16 derived spheroids. 5:1 E:T ratio was used for all target cell lines. (B) Automated live-cell imaging using Incucyte to detect pHNSCC #16 spheroids (red: mCherry⁺ pHNSCC #16 cells). E:T = effector:target cell ratio. Mean with standard deviation shown. Statistical analysis was performed using two-way ANOVA with Bonferroni's post-hoc test for comparison between full-length CAR-NK-92 cells and unmodified NK-92 cells at 12 h and 48 h. n = 6 (two separate transductions of NK-92 used, each assessed in triplicates). ** = $p < 0.01$, **** = $p < 0.0001$.

4. Discussion

HNSCC is a genetically complex, highly aggressive and relapse-prone form of cancer, requiring a multidimensional interplay of treatment regimens, in which immunotherapy has proven to play a pivotal role. In this study, we aimed to expand the immunotherapeutic tool kit to CAR-NK cell approaches against HNSCC. We present a functional CAR-NK-92 cell strategy targeting HER1 that was successfully tested against SCC-4 and SCC-25 as well as EpCAM sorted and expanded pHNSCC cells in 2D and 3D killing assays.

To develop representative in vitro models of HNSCC, single tumor cells were isolated from inner tumor masses and characterized. High percentages of CD45⁺ immune cells were observed in 6 out of 9 samples, supporting HNSCC as one of the most infiltrated tumors [21]. Our flow cytometry and IHC data also support previous single-cell transcriptomic analysis, which identified 40% malignant and 60% non-malignant cells in 18 HNSCC samples [22]. Further investigation of the non-malignant population showed the presence of T cells, B cells, macrophages, monocytes, endothelial cells and fibroblasts. The composition of these non-malignant cell populations varied depending on tumor type, location, HPV status and genetic aberrations. Furthermore, HNSCC tumors were found to have one of the highest numbers of infiltrated, cytotoxic NK cells present, which correlated with improved overall survival due to the immune cell-mediated anti-tumor activity [21]. However, T cell populations also displayed exhaustion markers, which varied strongly among patient samples, suggesting an immunosuppressive TME, which may limit efficacy of immunotherapeutic approaches [22]. In this study, we did not characterize the immune cells to allow further conclusions. Generally, a high presence of immune cells, specifically NK cells and macrophages, correlates with better prognosis and validates investigations of immunotherapeutic approaches for these tumors [23].

Expression patterns of HER1, CD44v6 and CD133 on freshly isolated pHNSCC samples showed HER1 had the highest expression of the three, reinforcing our choice as a therapeutic target and supporting previous literature showing over 80% HER1 expression. CD133 displayed the lowest expression, as expected from previous work that described CD133 as a putative cancer stem cell marker and CD133⁺ cells as a rather rare subpopulation [24]. The CD45[−] population consisted of a large portion of EpCAM⁺ cells and as epithelial cells are the cell-of-origin for this type of tumor, we sorted freshly isolated pHNSCC samples for EpCAM as described by others and expanded the samples in an epithelial cell-specific medium [20]. This procedure helped avoid fibroblast overgrowth in cell culture flasks without the need to use the partial trypsinization method over weeks to months with a success rate below 25% [20,25]. After EpCAM⁺ sorting, HER1 expression reached over 50% in 5 out of 7 freshly isolated patient samples. Overall, this allowed us to create pHNSCC-derived cell lines, which persisted in culture for months with consistent epithelial morphology (Supplementary Figure S4), allowing freeze/thaw cycles and transduction with lentiviral vectors (e.g., for mCherry expression). This isolation and culture strategy generated a sufficient number of cells from primary material, which enabled us to conduct different experiments using the same pHNSCC cell line.

To further characterize EpCAM sorted and expanded pHNSCC samples, we conducted OGM, which alongside SCC-4 and SCC-25 cell lines, displayed the highly heterogeneous background and genetic complexity of the disease. SCC-4 cells showed the highest number of genomic aberrations, which may explain the higher E:T ratio needed to effectively kill these cells compared to SCC-25 and pHNSCC cells and suggests that SCC-4 cells may reflect a rather resistant model of HNSCC for this type of therapy. However, all cell lines also shared a high-fold amplification of chromosomal region 11q13, which encodes genes involved in cell cycle control that are regarded as oncogenic drivers, such as *CCND1*, *FADD* and *CTTN* [18]. This also supports the finding that pHNSCC samples that harbor gene amplification of chromosomal region 11q13, which serves as a marker for poor prognosis, were more likely to form stable cell lines [26].

To establish a functional anti-HER1 CAR-NK cell strategy, a triple parameter reporter (TPR) cell line was used to test our CAR construct for tonic signaling, and showed signaling

for 7D6 CH3 in the absence of target antigen, which can lead to exhaustion in CAR-T cells (Supplementary Figure S3) [27,28]. From the remaining CAR candidates, we selected 12D3 CH3 and 2F8 CH3 as the best candidates to compare two different scFvs in all further experiments. These two most promising full-length CAR candidates outperformed all controls in enhanced cytotoxic killing against SCC-4, SCC-25 and both pHNSCC cell lines. Additionally, both full-length CAR-NK-92 cells demonstrated enhanced apoptosis induction in all target cells as well as increased CD107a expression, indicating degranulation of granzyme and perforins as mechanisms of apoptosis induction [29,30]. Another main function of NK cells is the recruitment and activation of other immune cells, such as monocytes, T cells and B cells to elicit an adaptive immune response, which is induced by enhanced secretion of IFN γ . These two full-length CAR-NK-92 cells exhibited IFN γ secretion upon co-culture with target cells SCC-4, SCC-25 and pHNSCC cell lines. Furthermore, IFN γ has also been shown to directly enhance NK cell-mediated induction of cancer cell death by apoptosis and cytolysis [31,32]. We also found enhanced cytotoxic killing of 3D spheroids using SCC-4, SCC-25 and pHNSCC cells in co-culture with both full-length CAR-NK-92 cells, confirming results from the 2D killing assays. For 3D models, higher E:T ratios were used for SCC-25 and pHNSCC cells to see an enhanced spheroid killing in co-cultures with full-length CAR-NK-92 cells, underlining more complex cellular interactions and most likely limited access to target antigens compared to 2D models, which results in increased treatment resistance as previously demonstrated [33].

Since strategies targeting single antigens can lead to resistance development, such approaches require close observation of tumor progression and resistance [34,35]. Therefore, we examined antigen expression profiles of remaining pHNSCC cells and found a strong reduction of HER1⁺ and CD44v6⁺HER1⁺ target cells, as expected, with increased CD44v6⁺ cells present after 24 h co-culture with full-length CAR-NK-92 cells. This may indicate expansion of clonal subsets as a response to CAR treatment, specifically the potential of cells that may resemble cancer stem cells to spread and repopulate. Antibodies against CD44v6 were shown to prevent such outgrowth in rat models of metastatic cancer [36]. Treatment resistance is another concern, as patients treated with cetuximab developed resistance to cetuximab as well as decreased responses to PD-1 checkpoint inhibitors in subsequent treatments [37]. It is well-known that other receptors of the ErbB family or downstream signaling molecules can compensate for the inhibition of one receptor [38], further supporting the idea of dual-targeted CAR-NK cell approaches. A previous study demonstrated enhanced and specific killing of primary HNSCC cells using CAR-T cells targeting CD44v6 [39]. A CAR strategy that targets both HER1 and CD44v6 using human T and NK cells may help to further eliminate putative cancer stem cell populations more completely, with the aim to reduce tumor escape and relapse incidences.

Another major drawback of adoptive cell therapy approaches is the upregulation of PD-L1 on target cells, which we also observed for SCC-4, SCC-25 and pHNSCC cells upon co-culture with unmodified and modified NK-92 cells (Supplementary Figure S5C) [40]. CAR-NK cell therapy may hence benefit from the combination of checkpoint inhibitors to prevent loss of immune cell functionality and aid in overcoming resistance in the immunosuppressive TME of HNSCC, which remains a challenge for any CAR therapeutic approach [41]. Further experiments are therefore required to assess performance of our anti-HER1 CAR-NK-92-cell strategy in a model that better recapitulates an immunosuppressive TME [42–44]. While further research is inevitable, HNSCC remains a disease that requires multimodal treatment regimens. Therefore, it is mandatory that new treatment strategies can be implemented into and further advance existing therapeutic strategies. Multiple studies have already shown beneficial outcomes of combined (CAR)-NK cell therapies and radiation or chemotherapy in other cancer models, making it a promising new therapeutic approach for HNSCC [45–48].

5. Conclusions

In the present study, CAR-NK-92 cells that target HER1 were generated and showed enhanced killing activity of SCC cell lines and established patient-derived pHNSCC cells in 2D and 3D co-culture models. Furthermore, improved IFN γ secretion and upregulated expression of CD107a were observed during co-culture with anti-HER1 CAR-NK-92 cells. However, characterization of remaining pHNSCC cells after co-culture with anti-HER1 CAR-NK-92 cells demonstrated an expansion of CD44v6⁺ cells, which may be indicative of a CSC-like phenotype. Together with the upregulated PD-L1 expression on pHNSCC cells after co-culture with anti-HER1 CAR-NK-92 cells, this suggests CAR-based approaches targeting a single tumor-associated antigen may not be suitable for monotherapy, and hence, may not be able to prevent high relapse rates and treatment resistance. Therefore, combined immunotherapeutic approaches that target multiple tumor-associated antigens as well as the immunosuppressive TME are essential to improve treatment responses and survival rates for HNSCC.

Supplementary Materials: The following supporting information can be downloaded at: <https://www.mdpi.com/article/10.3390/cancers15123169/s1>. Supplementary Figure S1: Characterization of SCC-4 and SCC-25 cell lines; Supplementary Figure S2. Enhanced IFN γ secretion of anti-HER1 CAR-NK-92 cells using E:T ratio 1:1 and 10:1. Supplementary Figure S3. Tonic signaling of anti-HER1 CAR-TPR cell line; Supplementary Figure S4. EpCAM expression on target cell lines; Supplementary Figure S5. Upregulation of PD-L1 on target cells upon NK-92 co-culture; Supplementary Figure S6. Immunohistochemistry staining of patient #16; Supplementary Figure S7. Immunohistochemistry staining of patient #15. Supplementary methods include Flow cytometry: surface marker expression and Immunohistochemistry staining and analysis (including Supplementary Table S1: Antibodies used in immunohistochemistry). File S1: Original Images of Western Blot.

Author Contributions: Conceptualization, M.M. and A.S.; experimental design: J.N., M.M. and K.Z.; methodology, J.N.; cloning and packaging: J.N.; functional CAR-NK cell assays: J.N.; WB: M.B. and M.M.; spheroid formation: I.K. and J.N.; primary materials: A.W., W.R. and A.A.; OGM: J.L.L. and D.S. (Doris Steinemann); IHC: L.N., J.-C.K. and M.P.K.; IHC software: D.S. (Dirk Schaudien); analysis: J.N.; writing original draft: J.N., M.M. and A.S.; writing—review and editing: all authors; supervision: M.M. and A.S.; funding acquisition: M.M., S.K., U.K. and A.S. All authors have read and agreed to the published version of the manuscript.

Funding: This research was funded by Deutsche Krebshilfe (70113658: S.K., M.M.) and the APC was funded by MHH Library.

Institutional Review Board Statement: The study was conducted in accordance with the Declaration of Helsinki, and approved by the Ethics Committee of Medizinische Hochschule Hannover /Hannover Medical School (No. 132 9573_BO_K2021, approved on 26 January 2021).

Informed Consent Statement: Informed consent was obtained from all subjects involved in the study.

Data Availability Statement: The data presented in this study are available in the article and Supplementary Material.

Acknowledgments: The authors thank the patients and their families for donating their tumor samples and Deutsche Krebshilfe for support of this project (70113658: S.K., M.M.). We would like to acknowledge the assistance of the Cell Sorting Core Facility at the Hannover Medical School supported in part by Braukmann-Wittenberg-Herz-Stiftung and Deutsche Forschungsgemeinschaft. Furthermore, we would like to thank Juliane Schott for the lentiviral mCherry vector, Peter Steinberger for providing us with their triple parameter reporter cell line and Christopher Batram and Marc Breuerle from Sartorius for their support and excellent guidance for the Incucyte device.

Conflicts of Interest: Author A.S. is listed as a co-author on a patent describing alpharetroviral vectors. No other authors declare any conflict of interest. The funders had no role in the design of the study; in the collection, analyses, or interpretation of data; in the writing of the manuscript; or in the decision to publish the results.

References

1. Bray, F.; Ferlay, J.; Soerjomataram, I.; Siegel, R.L.; Torre, L.A.; Jemal, A. Global cancer statistics 2018: GLOBOCAN estimates of incidence and mortality worldwide for 36 cancers in 185 countries. *CA Cancer J. Clin.* **2018**, *68*, 394–424. [[CrossRef](#)]
2. Ang, K.K.; Harris, J.; Wheeler, R.; Weber, R.; Weber, R.; Rosenthal, D.I.; Nguyen-Tân, P.F.; Westra, W.H.; Chung, C.H.; Jordan, R.C.; et al. Human Papillomavirus and Survival of Patients with Oropharyngeal Cancer. *N. Engl. J. Med.* **2020**, *363*, 24–35. [[CrossRef](#)]
3. Vermorken, J.B.; Mesia, R.; Rivera, F.; Remenar, E.; Kawecki, A.; Rottey, S.; Erfan, J.; Zabolotnyy, D.; Kienzer, H.-R.; Cupissol, D.; et al. Platinum-Based Chemotherapy plus Cetuximab in Head and Neck Cancer. *N. Engl. J. Med.* **2008**, *359*, 1116–1127. [[CrossRef](#)] [[PubMed](#)]
4. Kao, H.-F.; Lou, P.-J. Immune checkpoint inhibitors for head and neck squamous cell carcinoma: Current landscape and future directions. *Head Neck* **2019**, *41*, 1–18. [[CrossRef](#)] [[PubMed](#)]
5. Mei, Z.; Zhang, K.; Lam, A.K.; Huang, J.; Qiu, F.; Qiao, B.; Zhang, Y. MUC1 as a target for CAR-T therapy in head and neck squamous cell carcinoma. *Cancer Med.* **2020**, *9*, 640–652. [[CrossRef](#)] [[PubMed](#)]
6. Geldres, C.; Savoldo, B.; Hoyos, V.; Caruana, I.; Zhang, M.; Yvon, E.; Del Vecchio, M.; Creighton, C.J.; Ittmann, M.; Ferrone, S.; et al. T lymphocytes redirected against the chondroitin sulfate proteoglycan-4 control the growth of multiple solid tumors both in vitro and in vivo. *Clin. Cancer Res.* **2014**, *20*, 962–971. [[CrossRef](#)]
7. Tang, X.; Yan, Z.; Wenjie, L.; Qi, T.; Renjie, C.; Jin, Z.; Zhenqing, F. T cells expressing a LMP1-specific chimeric antigen receptor mediate antitumor effects against LMP1-positive nasopharyngeal carcinoma cells in vitro and in vivo. *J. Biomed. Res.* **2014**, *28*, 468–475. [[CrossRef](#)]
8. Robbins, Y.; Greene, S.; Friedman, J.; E Clavijo, P.; Van Waes, C.; Fabian, K.P.; Padget, M.R.; Sater, H.A.; Lee, J.H.; Soon-Shiong, P.; et al. Tumor control via targeting pd-1l with chimeric antigen receptor modified nk cells. *eLife* **2020**, *9*, e54854. [[CrossRef](#)]
9. Papa, S.; Adami, A.; Metoudi, M.; Achkova, D.; van Schalkwyk, M.; Pereira, A.P.; Bosshard-Carter, L.; Whilding, L.; van der Stegen, S.; Davies, D.; et al. A phase I trial of T4 CAR T-cell immunotherapy in head and neck squamous cancer (HNSCC). *J. Clin. Oncol.* **2018**, *36*, 3046. [[CrossRef](#)]
10. Papa, S.; van Schalkwyk, M.; Maher, J. Clinical Evaluation of ErbB-Targeted CAR T-Cells, Following Intracavity Delivery in Patients with ErbB-Expressing Solid Tumors. In *Gene Therapy of Solid Cancers—Methods and Protocols*; Walther, W., Stein, U., Eds.; Humana Press: Totowa, NJ, USA, 2015; Volume 1317, 387p. [[CrossRef](#)]
11. Lee, D.W.; Santomaso, B.D.; Locke, F.L.; Ghobadi, A.; Turtle, C.J.; Brudno, J.N.; Maus, M.V.; Park, J.H.; Mead, E.; Pavletic, S.; et al. ASTCT Consensus Grading for Cytokine Release Syndrome and Neurologic Toxicity Associated with Immune Effector Cells. *Biol. Blood Marrow Transplant.* **2019**, *25*, 625–638. [[CrossRef](#)]
12. Liu, E.; Tong, Y.; Dotti, G.; Shaim, H.; Savoldo, B.; Mukherjee, M.; Orange, J.; Wan, X.; Lu, X.; Reynolds, A.; et al. Cord blood NK cells engineered to express IL-15 and a CD19-targeted CAR show long-term persistence and potent antitumor activity. *Leukemia* **2018**, *32*, 520–531. [[CrossRef](#)] [[PubMed](#)]
13. Liu, E.; Marin, D.; Banerjee, P.; Macapinlac, H.A.; Thompson, P.; Basar, R.; Kerbauy, L.N.; Overman, B.; Thall, P.; Kaplan, M.; et al. Use of CAR-transduced natural killer cells in CD19-positive lymphoid tumors. *N. Engl. J. Med.* **2020**, *382*, 545–553. [[CrossRef](#)] [[PubMed](#)]
14. Williams, B.A.; Law, A.D.; Routy, B.; Denhollander, N.; Gupta, V.; Wang, X.-H.; Chaboureau, A.; Viswanathan, S.; Keating, A. A phase I trial of NK-92 cells for refractory hematological malignancies relapsing after autologous hematopoietic cell transplantation shows safety and evidence of efficacy. *Oncotarget* **2017**, *8*, 89256–89268. [[CrossRef](#)] [[PubMed](#)]
15. Wei, Q.; Sheng, L.; Shui, Y.; Hu, Q.; Nordgren, H.; Carlsson, J. EGFR, HER2, and HER3 expression in laryngeal primary tumors and corresponding metastases. *Ann. Surg. Oncol.* **2008**, *15*, 1193–1201. [[CrossRef](#)]
16. Zhang, J.; Saba, N.F.; Chen, G.; Shin, D.M. Targeting HER (ERBB) signaling in head and neck cancer: An essential update. *Mol. Asp. Med.* **2015**, *45*, 74–86. [[CrossRef](#)]
17. Suerth, J.D.; Labenski, V.; Schambach, A. Alpharetroviral vectors: From a cancer-causing agent to a useful tool for human gene therapy. *Viruses* **2014**, *6*, 4811–4838. [[CrossRef](#)]
18. Muller, D.; Millon, R.; Velten, M.; Bronner, G.; Jung, G.; Engelmann, A.; Flesch, H.; Eber, M.; Methlin, G.; Abecassis, J. Amplification of 11q13 DNA markers in head and neck squamous cell carcinomas: Correlation with clinical outcome. *Eur. J. Cancer* **1997**, *33*, 2203–2210. [[CrossRef](#)]
19. Schartinger, V.H.; Schmutzhard, J.; Wurm, M.; Schwentner, I.M.; Obrist, P.; Oberaigner, W.; Sprinzl, G.M. The expression of EGFR, HER2 and EpCam in Head and Neck squamous cell carcinomas. *memo Mag. Eur. Med. Oncol.* **2009**, *2*, 45–50. [[CrossRef](#)]
20. Owen, J.H.; Graham, M.P.; Chinn, S.B.; Darr, O.F.; Chepeha, D.B.; Wolf, G.T.; Bradford, C.R.; Carey, T.E.; Prince, M.E. Novel method of cell line establishment utilizing fluorescence-activated cell sorting resulting in 6 new head and neck squamous cell carcinoma lines. *Head Neck* **2016**, *38*, E459–E467. [[CrossRef](#)]
21. Mandal, R.; Şenbabaoglu, Y.; Desrichard, A.; Havel, J.J.; Dalin, M.G.; Riaz, N.; Lee, K.-W.; Ganly, I.; Hakimi, A.A.; Chan, T.A.; et al. The head and neck cancer immune landscape and its immunotherapeutic implications. *JCI Insight* **2016**, *1*, e89829. [[CrossRef](#)]
22. Puram, S.V.; Tirosh, I.; Parikh, A.S.; Patel, A.P.; Yizhak, K.; Gillespie, S.; Rodman, C.; Luo, C.L.; Mroz, E.A.; Emerick, K.S.; et al. Single-Cell Transcriptomic Analysis of Primary and Metastatic Tumor Ecosystems in Head and Neck Cancer. *Cell* **2017**, *171*, 1611–1624.e24. [[CrossRef](#)]

23. Sun, X.; Zhang, L.; Liu, S. The Immune Infiltration in HNSCC and Its Clinical Value: A Comprehensive Study Based on the TCGA and GEO Databases. *Comput. Math. Methods Med.* **2021**, *2021*, 1163250. [[CrossRef](#)] [[PubMed](#)]
24. Zhang, Q.; Shi, S.; Yen, Y.; Brown, J.; Ta, J.Q.; Le, A.D. A subpopulation of CD133+ cancer stem-like cells characterized in human oral squamous cell carcinoma confer resistance to chemotherapy. *Cancer Lett.* **2010**, *289*, 151–160. [[CrossRef](#)]
25. Heo, D.S.; Snyderman, C.; Gollin, S.M.; Pan, S.; Walker, E.; Deka, R.; Barnes, E.L.; Johnson, J.T.; Herberman, R.B.; Whiteside, T.L. Biology, cytogenetics, and sensitivity to immunological effector cells of new head and neck squamous cell carcinoma lines. *Cancer Res.* **1989**, *49*, 5167–5175. [[PubMed](#)]
26. White, J.S.; Weissfeld, J.L.; Ragin, C.C.; Rossie, K.M.; Martin, C.L.; Shuster, M.; Ishwad, C.S.; Law, J.C.; Myers, E.N.; Johnson, J.T.; et al. The Influence of Clinical and Demographic Risk Factors on the Establishment of Head and Neck Squamous Cell Carcinoma Cell Lines. *Oral Oncol.* **2007**, *43*, 701–712. [[CrossRef](#)]
27. Jutz, S.; Leitner, J.; Schmetterer, K.; Doel-Perez, I.; Majdic, O.; Grabmeier-Pfistershammer, K.; Paster, W.; Huppa, J.B.; Steinberger, P. Assessment of costimulation and coinhibition in a triple parameter T cell reporter line: Simultaneous measurement of NF- κ B, NFAT and AP-1. *J. Immunol. Methods* **2016**, *430*, 10–20. [[CrossRef](#)] [[PubMed](#)]
28. Long, A.H.; Haso, W.H.; Shern, J.F.; Wanhainen, K.M.; Murgai, M.; Ingaramo, M.; Smith, J.P.; Walker, A.J.; Kohler, M.E.; Venkateshwara, W.R.; et al. 4-1BB Costimulation Ameliorates T Cell Exhaustion Induced by Tonic Signaling of Chimeric Antigen Receptors. *Nat. Med.* **2015**, *21*, 581–590. [[CrossRef](#)]
29. Alter, G.; Malenfant, J.M.; Altfeld, M. CD107a as a functional marker for the identification of natural killer cell activity. *J. Immunol. Methods* **2004**, *294*, 15–22. [[CrossRef](#)]
30. Krzewski, K.; Gil-Krzewska, A.; Nguyen, V.; Peruzzi, G.; Coligan, J.E. LAMP1/CD107a is required for efficient perforin delivery to lytic granules and NK-cell cytotoxicity. *Blood* **2013**, *121*, 4672–4683. [[CrossRef](#)]
31. Cui, F.; Qu, D.; Sun, R.; Zhang, M.; Nan, K. NK cell-produced IFN- γ regulates cell growth and apoptosis of colorectal cancer by regulating IL-15. *Exp. Ther. Med.* **2019**, *19*, 1400–1406. [[CrossRef](#)]
32. Wang, R.; Jaw, J.J.; Stutzman, N.C.; Zou, Z.; Sun, P.D. Natural killer cell-produced IFN- γ and TNF- α induce target cell cytolysis through up-regulation of ICAM-1. *J. Leukoc. Biol.* **2012**, *91*, 299–309. [[CrossRef](#)] [[PubMed](#)]
33. Gopal, S.; Kwon, S.J.; Ku, B.; Lee, D.W.; Kim, J.; Dordick, J.S. 3D tumor spheroid microarray for high-throughput, high-content natural killer cell-mediated cytotoxicity. *Commun. Biol.* **2021**, *4*, 893. [[CrossRef](#)]
34. O’rourke, D.M.; Nasrallah, M.P.; Desai, A.; Melenhorst, J.J.; Mansfield, K.; Morrisette, J.J.D.; Martinez-Lage, M.; Brem, S.; Maloney, E.; Shen, A.; et al. A single dose of peripherally infused EGFRvIII-directed CAR T cells mediates antigen loss and induces adaptive resistance in patients with recurrent glioblastoma. *Sci. Transl. Med.* **2017**, *9*, eaaa0984. [[CrossRef](#)] [[PubMed](#)]
35. Park, J.H.; Rivière, I.; Gonen, M.; Wang, X.; Sénéchal, B.; Curran, K.J.; Sauter, C.; Wang, Y.; Santomasso, B.; Mead, E.; et al. Long-Term Follow-up of CD19 CAR Therapy in Acute Lymphoblastic Leukemia. *N. Engl. J. Med.* **2018**, *378*, 449–459. [[CrossRef](#)] [[PubMed](#)]
36. Günthert, U.; Hofmann, M.; Rudy, W.; Reber, S.; Zöller, M.; Haußmann, I.; Matzku, S.; Wenzel, A.; Ponta, H.; Herrlich, P. A New Variant of Glycoprotein CD44 Confers Metastatic Potential to Rat Carcinoma Cells. *Cell* **1991**, *55*, 13–24. [[CrossRef](#)]
37. Ferris, R.L.; Blumenschein, G.; Fayette, J.; Guigay, J.; Colevas, A.D.; Licitra, L.; Harrington, K.; Kasper, S.; Vokes, E.E.; Even, C.; et al. Nivolumab in Patients with Recurrent or Metastatic Squamous Cell Carcinoma of the Head and Neck: Efficacy and Safety in CheckMate 141 by Prior Cetuximab Use. *Clin. Cancer Res.* **2019**, *25*, 5221–5230. [[CrossRef](#)]
38. De Pauw, I.; Lardon, F.; Van den Bossche, J.; Baysal, H.; Fransen, E.; Deschoolmeester, V.; Pauwels, P.; Peeters, M.; Vermorken, J.B.; Wouters, A. Simultaneous targeting of EGFR, HER2, and HER4 by afatinib overcomes intrinsic and acquired cetuximab resistance in head and neck squamous cell carcinoma cell lines. *Mol. Oncol.* **2018**, *12*, 830–854. [[CrossRef](#)]
39. Haist, C.; Schulte, E.; Bartels, N.; Bister, A.; Poschinski, Z.; Ibach, T.C.; Geipel, K.; Wiek, C.; Wagenmann, M.; Monzel, C.; et al. CD44v6-targeted CAR T-cells specifically eliminate CD44 isoform 6 expressing head/neck squamous cell carcinoma cells. *Oral Oncol.* **2021**, *116*, 105259. [[CrossRef](#)]
40. Spranger, S.; Spaapen, R.M.; Zha, Y.; Williams, J.; Meng, Y.; Ha, T.T.; Gajewski, T.F. Up-regulation of PD-L1, IDO, and Tregs in the melanoma tumor microenvironment is driven by CD8+ T cells. *Sci. Transl. Med.* **2013**, *5*, 200ra116. [[CrossRef](#)]
41. Park, J.-E.; Kim, S.-E.; Keam, B.; Park, H.-R.; Kim, S.; Kim, M.; Kim, T.M.; Doh, J.; Kim, D.-W.; Heo, D.S. Anti-tumor effects of NK cells and anti-PD-L1 antibody with antibody-dependent cellular cytotoxicity in PD-L1-positive cancer cell lines. *J. Immunother. Cancer* **2020**, *8*, e000873. [[CrossRef](#)]
42. Paterson, K.; Paterson, S.; Mulholland, T.; Coffelt, S.B.; Zagnoni, M. Assessment of CAR-T Cell-Mediated Cytotoxicity in 3D Microfluidic Cancer Co-Culture Models for Combination Therapy. *J. Eng. Med. Biol.* **2022**, *3*, 86–95. [[CrossRef](#)] [[PubMed](#)]
43. Liu, W.N.; Fong, S.Y.; Tan, W.W.S.; Tan, S.Y.; Liu, M.; Cheng, J.Y.; Lim, S.; Suteja, L.; Huang, E.K.; Chan, J.K.Y.; et al. Establishment and characterization of humanized mouse NPC-PDX model for testing immunotherapy. *Cancers* **2020**, *12*, 1025. [[CrossRef](#)] [[PubMed](#)]
44. Liu, W.N.; So, W.Y.; Harden, S.L.; Fong, S.Y.; Wong, M.X.Y.; Tan, W.W.S.; Tan, S.Y.; Ong, J.K.L.; Rajarethinam, R.; Liu, M.; et al. Successful targeting of PD-1/PD-L1 with chimeric antigen receptor-natural killer cells and nivolumab in a humanized mouse cancer model. *Sci. Adv.* **2022**, *8*, eadd1187. [[CrossRef](#)] [[PubMed](#)]
45. Kim, K.W.; Jeong, J.-U.; Lee, K.-H.; Uong, T.N.T.; Rhee, J.H.; Ahn, S.-J.; Kim, S.-K.; Cho, D.; Nguyen, H.P.Q.; Pham, C.T.; et al. Combined NK cell therapy and radiotherapy exhibit long-term therapeutic and anti-metastatic effects in a human triple negative breast cancer model. *Int. J. Radiat. Oncol. Biol. Phys.* **2020**, *108*, 115–125. [[CrossRef](#)]

46. Walle, T.; Kraske, J.A.; Liao, B.; Lenoir, B.; Timke, C.; Halbach, E.v.B.U.; Tran, F.; Griebel, P.; Albrecht, D.; Ahmed, A.; et al. Radiotherapy orchestrates natural killer cell dependent antitumor immune responses through CXCL8. *Sci. Adv.* **2022**, *8*, eabh4050. [[CrossRef](#)]
47. Canter, R.J.; Grossenbacher, S.K.; Foltz, J.A.; Sturgill, I.R.; Park, J.S.; Luna, J.I.; Kent, M.S.; Culp, W.T.N.; Chen, M.; Modiano, J.F.; et al. Radiotherapy enhances natural killer cell cytotoxicity and localization in pre-clinical canine sarcomas and first-in-dog clinical trial. *J. Immunother. Cancer* **2017**, *5*, 98. [[CrossRef](#)]
48. Klapdor, R.; Wang, S.; Hacker, U.; Büning, H.; Morgan, M.; Dörk, T.; Hillemanns, P.; Schambach, A. Improved Killing of Ovarian Cancer Stem Cells by Combining a Novel Chimeric Antigen Receptor-Based Immunotherapy and Chemotherapy. *Hum. Gene Ther.* **2017**, *28*, 886–896. [[CrossRef](#)]

Disclaimer/Publisher’s Note: The statements, opinions and data contained in all publications are solely those of the individual author(s) and contributor(s) and not of MDPI and/or the editor(s). MDPI and/or the editor(s) disclaim responsibility for any injury to people or property resulting from any ideas, methods, instructions or products referred to in the content.